A New Method of Materials Characterization for a Complex System by Obtaining the Middle Range Ordering

Y.Waseda [a,*], S.Suzuki[a], and M.Saito[b]

[a] *Institute of Multidisciplinary Research for Advanced Materials, Tohoku University, 2-1-1 Katahira, Aoba-ku, Sendai, 980-8577, Japan*
[b] *School of Health Sciences, Faculty of Medicine, Niigata University, Niigata, Niigata 951-8518, Japan*

(Received August 12, 2004:final form August 25, 2004)

ABSTRACT

Middle range ordering is known to be of great importance for characterizing the structure of various substances in a variety of states. This is particularly true for a complex system. An attempt has been made to present a new method for obtaining information including middle range ordering. In this method, the realistic atomic scale model structure is estimated by fitting both the ordinary interference function and the environmental interference function obtained from anomalous X-ray scattering (AXS) data with model calculation using reverse Monte Carlo (RMC) simulation technique and then middle range ordering in the range of a few nanometers can be visualized. The usefulness of this new method has been demonstrated by some impressive results of molten CuBr and corrosion products (FeOOH) formed on the steel surface.

Keywords: middle range ordering, molten salt, ferric oxyhydroxide, anomalous X-ray scattering, reverse Monte Carlo simulation

1. INTRODUCTION

There has been a vast amount of research on new materials and a better understanding of the physical and chemical properties of these new materials is known to depend heavily upon their structural characterization at a microscopic level. In the crystals, all atomic distribution characterized by the long range ordering can be described when we introduce a few parameters of position and distance. Such a simple definition is impossible in both the liquid and glassy states, but their atomic distributions in the near-neighbor region are known to be characterized using the concept of the short-range ordering /1/.

On the other hand, one can frequently find a system of interest which is not classified into these two categories. For example, the structure with non-periodicity is confirmed in the second-generation amorphous alloys called "bulk amorphous alloys"/2/, but rather complex structural features are also recognized. This is partly attributed to their compositions, which always contain several types of atoms, at least three components. Then, information about their middle range ordering is strongly required for materials characterization of bulk amorphous alloys. The structural feature of corrosion products, which are mainly ferric oxyhydroxides with some alloying elements, is found to be very complicated /3/, and some parts of these corrosion products have been assigned to the amorphous state /4/. This again suggests the middle-range ordering to be of great importance for characterizing the structure of corrosion products. However, an established method has not yet been given for describing the middle range ordering. An idea for obtaining the partial structures in a binary disordered

* Corresponding author. Tel/Fax +81-22-217-4814; e-mail: waseda@tagen.tohoku.ac.jp

system has been proposed by fitting the experimental interference functions with model calculation using the reverse Monte Carlo (RMC) simulation technique /5,6/. Some successful results with molten salts /7,8/ and metallic liquid alloys /9/ prompt us to extend this idea to a complex system.

The purpose of this paper is to describe one way to obtain the middle-range ordering in a few nanometers for a complex system including the results of corrosion products formed on the steel surface /10,11/.

2. FUNDAMENTALS OF A NEW METHOD

An idea for obtaining the middle range ordering in a system of interest is to estimate the realistic atomic scale model structure by fitting two or three independent experimental data with model calculation using the reverse Monte Carlo (RMC) simulation technique. For example, the atomic distribution in the region of a few nanometers can be estimated by fitting both the ordinary interference function and the environmental interference function obtained from the anomalous X-ray scattering (AXS) coupled with the reverse Monte Carlo (RMC) simulation technique /7-11/. The resultant atomic distribution is considered to be, at least as regards the necessary condition, best for explaining two or three independent experimental data, although it might not be the sufficient condition /12/. The essential points of this new method are given below.

Quantitative description of the atomic arrangements in non-crystalline system featured by the short range ordering usually employs the radial distribution function (hereafter referred to as RDF) that gives the probability of finding another atom from an origin atom as a function of radial distance /1/. This RDF can be simply extended to a crystalline system given by the long range ordering, so that it is worth mentioning that the RDF concept does give an almost unique way to present the middle range ordering without any change in its principle.

On the other hand, the environment of each atom differs from those of other atoms in both crystalline and non-crystalline systems including more than two components. This frequently makes the interpretation of their RDF data not so easy /13-15/. For this purpose, the near neighbor atomic correlation of the individual chemical constituents or the local chemical environment around a specific element is needed for materials characterization of multi-component systems. The anomalous x-ray scattering (hereafter referred to as AXS) method, by using the so-called anomalous dispersion effect near the absorption edge of the constituent elements, has recently received much attention, because its usefulness and validity were recognized for providing information about the local chemical environment of a specific element without any assumption for many more elements in the periodic table /12/. The availability of the intense white x-rays produced from synchrotron radiation also greatly improved both acquisition and quality of the AXS data by enabling the use of an energy in which the anomalous dispersion effect is the greatest. It would be the present authors' intention to employ the experimental interference functions obtained from both conventional and anomalous x-ray scattering in order to get information of the middle range ordering. The method for analyzing the measured AXS intensity data has been described in detail /7,12/ and only some essential points are given below, using the case of a binary non-crystalline system.

The reduced interference function, $i(Q,E)$ for a binary non-crystalline system can be given as follows /7/,

$$i(Q,E) \equiv I(Q,E) - \sum_i c_i f_i^2(Q,E) = \sum_{i=1}^{2}\sum_{j=1}^{2} c_i c_j f_i(Q,E) f_j(Q,E)\{a_{ij}(Q)-1\} \quad (1)$$

where c_i is the atomic fraction, $I(Q,E)$ is the coherent x-ray scattering intensity which corresponds to the structurally sensitive part of the total scattering intensity and $f_i(Q,E)$ is the atomic scattering factor of i-component, Q and E are the wave vector and the incident x-ray energy, respectively. On the other hand, $a_{ij}(Q)$ is the Faber-Ziman's type partial structure factors of i-j pair /16/ and it is connected with the partial pair distribution function $g_{ij}(r)$ in the following Fourier transform:

$$a_{ij}(Q) = 1 + \frac{4\pi\rho_0}{Q}\int_0^\infty r[g_{ij}(r)-1]\sin(Qr)dr, \quad (2)$$

where ρ_0 is the average number density in the system.

As seen in eq. (1), the coefficients of $\{a_{ij}(Q)-1\}$

depend on the atomic scattering factors and concentrations, so that the partial structure factors, $a_{ij}(Q)$, can be determined from three independent scattering experiments for which the coefficients are altered. The use of anomalous dispersion effect detected in the close vicinity of the absorption edge relevant to K- or L-shell electrons of a constituent is one way to vary the atomic scattering factors.

When the energy of the incident x-ray beam is close to the absorption edge of the constituent elements, the atomic scattering factor should be expressed in the following form /17/,

$$f(Q,E) = f^0(Q) + f'(E) + if''(E) \tag{3}$$

where $f^0(Q)$ corresponds to the scattering factor of the constituent element at the energy sufficiently away from the absorption edge. The values of $f'(E)$ and $f''(E)$ are the real and imaginary components of the so-called anomalous dispersion terms, respectively.

At the lower energy side of the absorption edge, the $f'(E)$ value gives a drastic change and the absolute values of $f''(E)$ and their energy-variation are quite small. For these reasons, a distinct energy variation of $f'(E)$ at the lower energy side of the absorption edge is convenient to the AXS measurement. It may be added as one of the advantages for the AXS method in the following. Since the absorption edge of any element is separated at least by several hundred eV, sufficient atomic sensitivity could be detected even in a system containing next neighboring elements of the periodic table /12/.

When the incident x-ray energies of E_1 and E_2 are tuned in the lower energy side of the absorption edge E_{abs} of A-element in an *A-B* binary system, the energy variation in intensity, $\Delta i_A(Q,E_1,E_2)$, should be attributed mainly to a change in the real part of anomalous dispersion terms of the component *A*. Then, the following simple relation can readily be given.

$$\begin{aligned}\Delta i_A(Q,E_1,E_2) = & \frac{\left\{I(Q,E_1) - \left\langle f^2(Q,E_1)\right\rangle\right\} - \left\{I(Q,E_2) - \left\langle f^2(Q,E_2)\right\rangle\right\}}{c_A\left\{f'_A(E_1) - f'_A(E_2)\right\}W(Q,E_1,E_2)} \\ = & \frac{c_A\Re\left\{f_A(Q,E_1) + f_A(Q,E_2)\right\}}{W(Q,E_1,E_2)}(a_{AA}(Q)-1) \\ & + \frac{c_B\Re\left\{f_B(Q,E_1) + f_B(Q,E_2)\right\}}{W(Q,E_1,E_2)}(a_{AB}(Q)-1)\end{aligned} \tag{4}$$

$$W(Q,E_1,E_2) = \sum_{k=A,B} c_k\Re\left\{f_k(Q,E_1) + f_k(Q,E_2)\right\}, \tag{5}$$

where $E_1 < E_2 < E_{abs}$ and $\Re$ denotes the real part of the values in the brackets. The quantity of $\Delta i_A(Q,E_1,E_2)$ contains two partial structure factors, $a_{AA}(Q)$ and $a_{AB}(Q)$. Similarly, $\Delta i_B(Q,E_3,E_4)$ includes $a_{BB}(Q)$ and $a_{AB}(Q)$. In other words, $\Delta i_A(Q,E_1,E_2)$ in eq. (4) corresponds to the environmental interference function contributed from the structure related only to the A-element and the terms in the front of $\{a_{kA}(Q)-1\}$ are the effective weighting factors. Then, the environmental interference function can be extended to the generalized form and it is connected with the pair distribution function as follows /12/:

$$\begin{aligned}\Delta i_A(Q,E_1,E_2) = & \sum_k \frac{c_k\Re\left\{f_k(Q,E_1) + f_k(Q,E_2)\right\}}{W(Q,E_1,E_2)}\left(\frac{1}{Q}\right) \\ & \times \int_0^\infty 4\pi r\rho_0\left\{g_{Ak}(r)-1\right\}\sin(Qr)dr\end{aligned} \tag{6}$$

Since the effective weighting factors for the radial distribution function are usually approximated to an average value in the range of Q space, the environmental radial distribution function around *A*, $4\pi r^2\rho_A(r)$, could be described in the following form.

$$4\pi r^2\rho_A(r) = 4\pi r^2\rho_0 + \frac{2r}{\pi}\int_0^\infty Q\Delta i_A(Q)\sin(Qr)dQ \tag{7}$$

The idea of the environmental structure function around a specific element is found to be quite effective for discussing the structure/property relationships without carrying out the complete separation of all partial functions. This is particularly true in multi-component non-crystalline systems containing more than three elements /12/. It is also worth mentioning that the basic concept of the partial structure is perfectly unchanged in the environmental structure function analysis. For example, there are six possible atomic pairs, A-A, A-B, A-C, B-B, B-C and C-C in the A-B-C ternary system. Then, the ordinary RDF is reflected on these six partial structures, whereas the environmental RDF around A obtained by the AXS measurement near

the absorption edge of A contains three partials of A-A, A-B and A-C. Thus, a relatively easy interpretation of the results can be allowed.

3. THE MIDDLE RANGE ORDERING IN MOLTEN CuBr

Noble metal halides such as CuBr are known to show a superionic conducting phase, where the anions form a body-centered cubic lattice whereas the cations are almost randomly distributed within the space among the anions /18/. This suggests that the structure of cation-cation (Cu-Cu) pairs is fairly structureless and different from those found in molten alkali halides such as NaCl. In order to reveal such characteristic features, the partial structure factors of Cu-Cu pairs and the middle range ordering in molten CuBr are strongly requested and then the AXS measurements in the transmission mode for molten CuBr were carried out with synchrotron radiation at a 7C beam line with a Si(111) double-crystal monochromator covering the energies ranging between 4 and 21 keV in the Photon Factory, Institute of Materials Structure Science, High-Energy Accelerator Organization, Tsukuba, Japan /7/.

The molten CuBr sample was filled into a devised quartz cell through tubes with a spacing of 50μm sandwiched between two quartz windows (10×20 mm^2 and 100μm thickness). The sample was heated at a temperature of 810±5 K, corresponding to 45 K above the melting point and the sample reservoir was encased with nickel for trapping CuBr vapor from the reservoir. This sample cell was set in a high temperature chamber /7/. Other details of the experimental procedure have already been reported /7,12/ and are not duplicated here.

Figure 1 shows the coherent X-ray intensity profiles of molten CuBr in electron units per atom. These intensity profiles were obtained from the measurements at four energies of 8.680, 8.955, 13.170 and 13.445 keV, which are 300 and 25eV below the Cu-K (8.980 keV) and Br-K (13.470 keV) absorption edges, respectively. The intensity profile was also obtained with the incident x-ray energy of 17.0 keV, which is far from two edges and the result is included in Fig. 1. The remarkable energy dependence in intensity is clearly detected and such variation should be attributed to the change in the

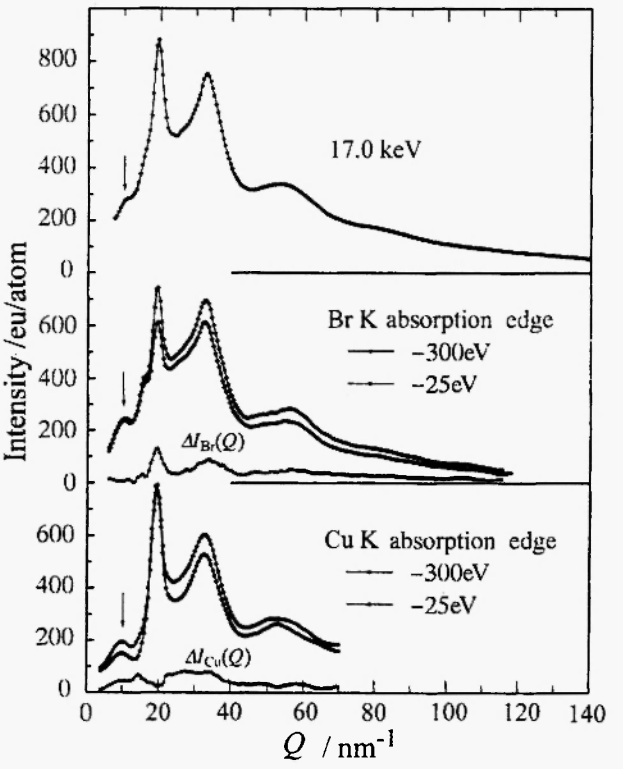

Fig. 1: Coherent intensity profiles of molten CuBr at 810 K in electron units per atom measured at incident energies of 8.680, 8.955, 13.170, 13.445 and 17.0 keV /7/.

anomalous dispersion effects of Cu and Br. Numerical examples of the $f'(E)$ value are –3.062 at 8.680 keV and –5.578 at 8.955 keV for Cu and –3.366 at 13.170 keV and –5.815 at 13.445 keV for Br, respectively. The normal atomic scattering factors are taken from the compilation of *International Tables for X-ray Crystallography* /19/. The atomic number density of the molten CuBr used is 36.3 atoms/nm^3, which is taken from the value of its molar volume /20/.

It is worth mentioning that a small pre-peak denoted by an arrow is also recognized in all three profiles of Fig. 1. Such pre-peak has already been observed in molten noble metal halides including CuBr /21/. The energy dependence of this pre-peak intensity at the Cu-K absorption edge is found to be distinct in comparison with the Br K absorption edge case. For this reason, when this correlation distance attributed to the pre-peak is assumed to be the Cu-Cu pairs without any further long-range atomic correlation of Cu, the corresponding

scattering intensity may be approximated by the relation of $I_{CuCu}(Q) \doteq \sin(Q\, r_{CuCu})/(Q\, r_{CuCu})$. In this case, the peak position of Q reflects the maximum of the $(Q\, r)$ function. On the other hand, an empirical rule of $(Q \cdot r) = 2.5\pi$ is suggested in various liquid alloys with respect to the relationship between the correlation length r in real space and the peak position Q in the intensity profile /22/. According to this empirical result, the pre-peak position found in molten CuBr suggests the corresponding correlation length of 0.79 nm. This implies that a particular density fluctuation of the order of 0.8 nm for Cu is quite likely to exist in molten CuBr /7/.

The environmental interference functions $Q\Delta i_{Cu}(Q)$ for Cu and $Q\Delta i_{Br}(Q)$ for Br are provided in Fig. 2 together with the ordinary interference function of $Qi(Q)$. Three partial structure factors of $a_{CuBr}(Q)$, $a_{BrBr}(Q)$ and $a_{CuCu}(Q)$ were estimated directly from the

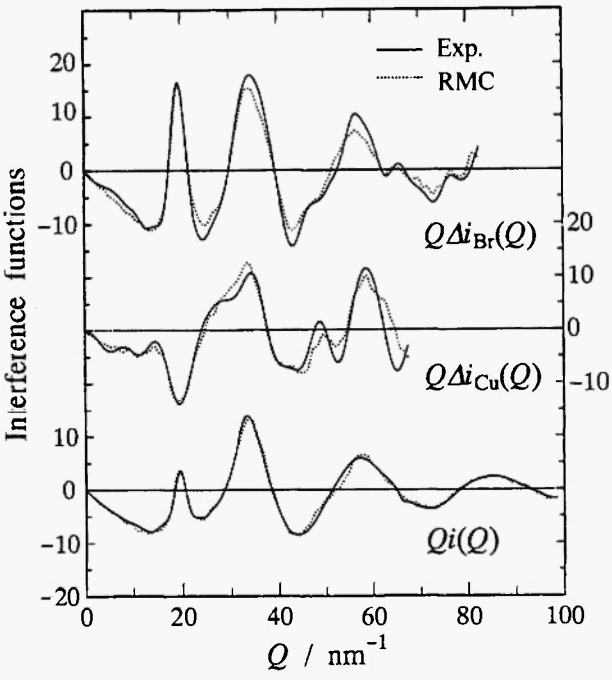

Fig. 2: The ordinary interference function $Qi(Q)$ and the environmental interference functions $Q\Delta i_{Br}(Q)$ and $Q\Delta i_{Cu}(Q)$ of molten CuBr. Solid lines correspond to the experimental data. Dotted lines denote values computed by the RMC simulation technique.

experimental data of Fig. 2 by solving the simultaneous linear equation /12-15/ and some interesting results are obtained /7/. For example, the first valley of $a_{CuBr}(Q)$ is located at Q value where the principal peak in $a_{BrBr}(Q)$ is situated and the partial structure factor of $a_{CuCu}(Q)$ indicates a particular structureless feature which is similar to the molten CuCl case /23,24/. However, it should be stressed here that the resultant partial structure factors are rather widely spread in certain positions and such behavior is frequently found mainly due to the experimental uncertainty and then the unpredictable large fluctuation in numerical solution, when the pivot of matrix is close to zero /25/. Such small experimental errors cannot always be excluded within the best knowledge of the present authors. For these reasons, some reservations should be made with respect to the quantitative accuracy of the partial structure factors obtained directly from the AXS data. This is particularly true from a standard mathematical point of view, although an improvement in reliability for further AXS measurements might be gained by increasing the normalized determinant proposed by Edwards *et al.* /15/. At the present moment it is still far from ideal /12/. For this reason, the present authors rather take the view that the realistic atomic structure should be estimated in order to reproduce the experimental AXS data and satisfy known physical constraint, as employed in the pioneer work on the partial structure of liquid Cu_6Sn_5 by Enderby *et al.* /13/. For this purpose, it may be safely said that the reverse Monte Carlo (hereafter referred as RMC) simulation technique /5,6/ is one of the useful methods. The results for molten CuBr are as follows.

We used the RMC simulation technique in the way essentially identical to that originally proposed by McGreevy and Pusztai /5/ with an initial configuration of 1728 particles; half of them represent Cu^+ ions, the remaining half Br^- ions, in a cubic box of size $L = 3.624$ nm for the molten CuBr case. The usual periodic boundary conditions are employed and the partial pair distribution functions, $g_{ij}(r)$, are computed. By applying the Fourier transformation to $g_{ij}(r)$, the interference functions via structure factors are compared with the experimental AXS data of Fig. 2 by estimating the following statistic.

$$\chi^2 = \sum_{m=1}^{n} \frac{\left\{i(Q_m) - i^c(Q_m)\right\}^2}{\sigma^2(Q_m)} + \sum_{\alpha}\sum_{m=1}^{n} \frac{\left\{\Delta i_\alpha(Q_m) - \Delta i_\alpha^c(Q_m)\right\}^2}{\sigma_\alpha^2(Q_m)} \quad (8)$$

where $i^c(Q_m)$ and $\Delta i_\alpha^c(Q_m)$ are the calculated interference function and its difference for α component, measured at Q_m, respectively. In addition, $\sigma(Q_m)$ and $\sigma_\alpha(Q_m)$ are the estimates of the experimental uncertainty. Then, a new configuration is generated through the random movement of one particle in a computer. It may be cited that the cut-off distance was set for each $g_{ij}(r)$ closer than the direct contact value of two particles, in order to prevent particles from approaching un-physically close to one another. When the new configuration violates these cut-off restrictions, it is rejected and the previous configuration data are restored. Otherwise the variation in $g_{ij}(r)$ is computed, and from this new $i^c(Q)$, $\Delta i^c(Q)$ and χ^2 are estimated. Figure 3 shows the flow chart of the RMC technique.

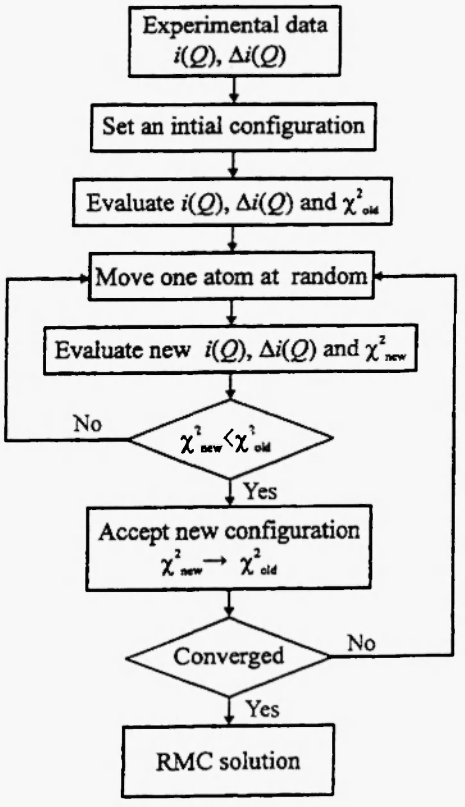

Fig. 3: Flow chart of the RMC simulation technique for analyzing the AXS data.

When the new value of χ^2 is smaller than the old one, the new configuration is accepted; otherwise it is accepted only with a probability less than unity. Such an iteration process is carried out until χ^2 indicates a reasonable convergence.

As shown in Fig. 2, the resultant RMC simulation results can reproduce well three independent interference functions of $Q\Delta i_{Cu}(Q)$, $Q\Delta i_{Br}(Q)$ and $Qi(Q)$. This agreement clearly suggests that the present approach basically works well. For convenience, the resultant three partial pair distribution functions of molten CuBr are also given in Fig. 4 and the following interesting points are suggested.

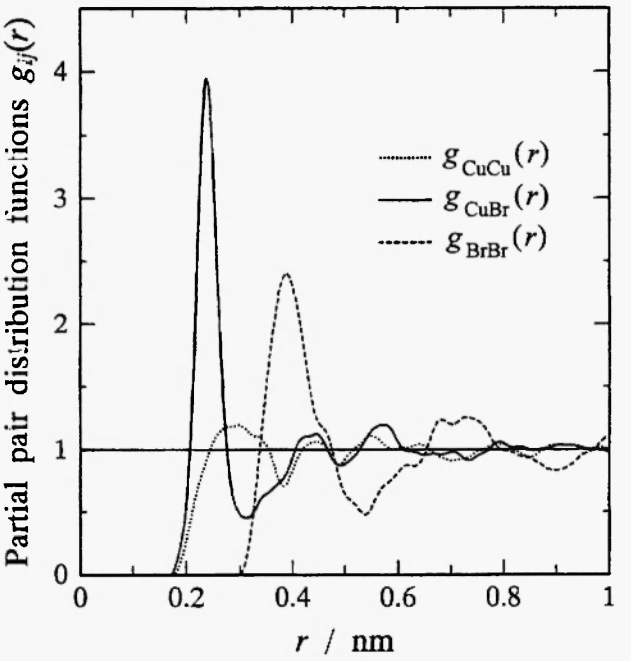

Fig. 4: The three partial pair distribution functions of molten CuBr.

The closest Cu-Cu distance is significantly smaller than that for Br-Br, indicating the like-ion penetration into the first unlike-ion coordination shell. An attempt was made to replace the Cu-Cu closest distance with the same value of the Br-Br case; however such modification gave gross disagreement between the experimental data and the calculated values. The coordination numbers for Cu-Br and Br-Br pairs can be estimated 3.1 at the distance of 0.245 nm and 11.4 at the distance of 0.398 nm on the average, respectively. It is

interesting that these values are closer to those for low-temperature phase of γ-CuBr, where the anions form a fcc lattice, than the high-temperature superionic phase of α-CuBr possessing a bcc sub-lattice. The integration of $r^2 g_{CuCu}(r)$ up to the first minimum in $r^2 g_{CuBr}(r)$ provides 1.2 Cu^+ ions penetrating to the first unlike-ion coordination shell. Such characteristic penetration behavior may be interpreted by a decrease in the Coulombic repulsion force interacting between Cu^+ ions due to the reduced charge transfer between unlike ions.

It is worth mentioning that the RMC simulation technique is not a unique mathematical procedure. Nevertheless, the resultant model structure obtained by fitting three independent experimental data is considered, at least, in a sense of the necessary condition at best although they might be not the sufficient condition. Then, one can use the resultant model structure for discussing the structural features including the middle range ordering within the framework of this physical constraint. Figure 5 shows a projection of the atomic positions in a 1.2 nm thick section obtained from a representative configuration obtained in the RMC simulation process. Here, each like-ion distribution is drawn separately at the bottom of Fig. 5 and bonds between like-ions are also drawn as sticks in order to emphasize the homogeneity in the

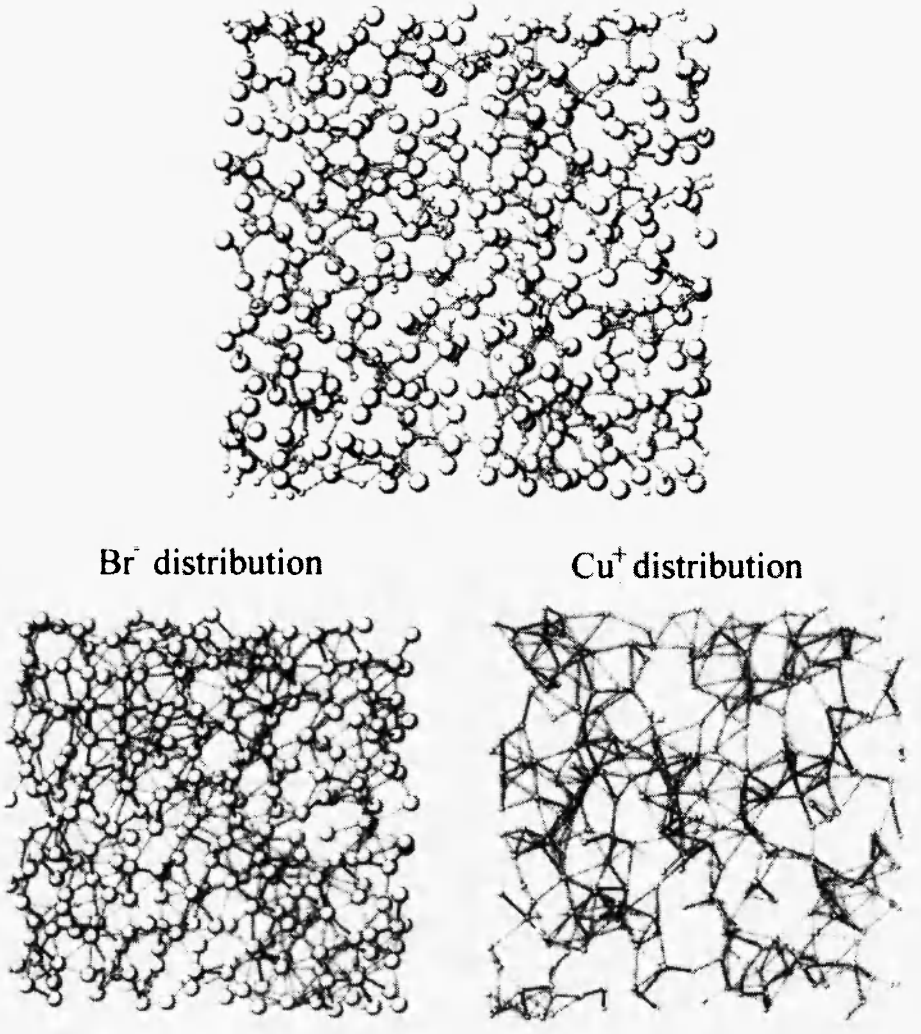

Fig. 5: A projection of the atomic positions in a 1.2 nm-thick section from a representative RMC-generated configuration. Larger atoms are Br, smaller atoms are Cu. Cu-Br bonds denoted by the distance up to the first minimum of $r^2 g_{CuBr}(r)$.

partial structures.

The distribution of Cu^+ ions is found to be less uniform and much sparser, whereas the distribution of Br^- ions is relatively uniform. The particular structural feature of the Cu^+ ion distribution gives the local cation density fluctuations with the length scale of about 0.8 nm. It is mentioned again that the pre-peak detected in intensity curves (see Fig. 1) at about $Q = 10$ nm^{-1} might have originated from such Cu^+ distribution.

From a representative configuration obtained in the RMC simulation process, the orientational three-particle correlation in molten CuBr can be estimated by calculating the bond angle distribution defined as the number of angles between the two vectors joining a central atom with any two neighbors of its coordination shell. The results are given in Fig. 6. The bond angle distribution in Br-Br-Br is characterized by two peaks occurring at approximately 60° and 110° (see Fig. 6). Combining the coordination number with the bond angle distribution, a close packed atomic configuration could be suggested for describing the anion-anion correlation in molten CuBr. The bond angle distribution in Br-Cu-Br indicates a single peak located at around

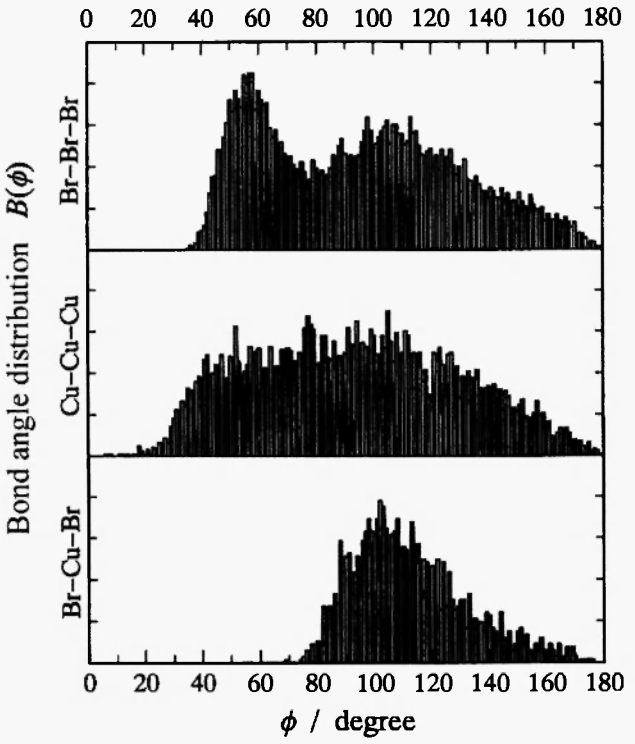

Fig. 6: Bond angle distributions of molten CuBr within the first coordination shell.

102°, which is not far from the ideal intra-tetrahedral angle of 109.3°. This suggests that tetrahedral coordination of Br^- ions around Cu^+ ions is quite likely to be a fundamental local ordering unit structure in molten CuBr. On the other hand, no specific feature is found in the bond angle distribution for Cu-Cu-Cu and it suggests only a very weak correlation. Considering all the results obtained in this work, the structure of molten CuBr can be described as a disordered close packing of Br^- ions, where the Cu^+ ions take strongly disordered distribution by meandering through essentially tetrahedral holes.

This conclusion could be drawn only from the realistic atomic scale model structure including the middle range ordering estimated by fitting three independent experimental data using the RMC simulation technique.

4. THE MIDDLE RANGE ORDERING IN CORROSION PRODUCTS FORMED ON THE STEEL SURFACE

Quantitative characterization of the atomic scale structure of corrosion products (frequently referred to as rust) is of great importance, because corrosion process of steel is known to be severely affected by the variety of state of corrosion products formed on the steel surface. For example, the corrosion rate of steel substrate in atmosphere is found to considerably reduce when the rust layer containing some small amount of alloying elements covers the steel surface as a protective film. However, the structure of corrosion products, which are ferric oxyhydroxides with some alloying elements, is not so simple and they are rather classified into a complex system. Since the corrosion products are formed by reaction of metallic elements, mainly iron, with oxygen and water originating from atmosphere, their structure appears to be severely affected by conditions. The corrosion products are found to consist of various components such as α-FeOOH, β-FeOOH, γ-FeOOH and Fe_3O_4 /3,26/. For these reasons, the crystallographic structure with the long range ordering is not sufficiently confirmed and some parts of steel rust are frequently assigned to the amorphous state characterized by the short range ordering /4/.

Several methods, such as electron probe micro-analysis, infrared spectroscopy, Raman spectroscopy, Mössbauer spectroscopy and EXAFS analysis have been applied, in order to characterize the structure, chemical composition and morphology of corrosion products formed on the steel surface under various conditions /26-32/. The results provided some interesting and important information on their composition and structure. Particularly, the EXAFS results /31,32/ suggest the local ordering unit structure of corrosion products is represented mainly by the FeO_6 octahedral unit structure and the linkage of such FeO_6 octahedra is, more or less, distorted by chromium addition. In addition, hydrogen atoms are quite likely to be intercalated in these structure units. However, some reservations have been stressed regarding information about linkage of the FeO_6 octahedral unit structure, because the EXAFS data result only from the near neighbor atomic arrangements. This strongly suggests the great importance of the middle range ordering for characterizing the corrosion products. The use of the AXS method coupled with the RMC simulation technique has brought about a significant breakthrough in this subject.

Some details of sample preparation and measurements are as follows. Five samples of iron, iron-2.0 mass% chromium, iron-3.0 mass% nickel and iron-1.6 mass% copper alloys were prepared from pure iron, chromium, nickel and copper by vacuum induction melting. These samples are hereafter referred to as Fe, Fe-2%Cr, Fe-3%Ni and Fe-1.6%Cu, respectively. A commercial weathering steel referred to as WS, of which the chemical composition is 0.10%C, 0.050%Si, 0.50%Mn, 0.096%P, 0.016%S, 0.15%Ni and 0.56%Cr in mass%, was also employed. These samples were shaped to10 mm square sheets of 1 mm in thickness and they were leached in artificial seawater with 2.5 mass% NaCl, 1.1 mass% $MgCl_2$, 0.4 mass% Na_2SO_4 and 0.07 mass% KCl at room temperature for about 15 days, so as to form colloidal corrosion products, from which powder rust samples were obtained by filtering.

Conventional diffraction experiments were carried out using Cu Kα radiation, in order to identify constituents of the corrosion products, and precise diffraction measurements were also made using Mo Kα radiation, which was generated at a power of 18 kW by Rigaku RINT-2000 with a graphite monochromator located on the diffracted beam line. AXS measurements were performed for estimating the environmental interference function for Fe in the corrosion products at BL-7C of Photon Factory, High Energy Accelerator Research Organization. The incident x-ray energies were tuned at 7.086 and 6.811 keV. These energies correspond to 25 and 300 eV below the Fe K absorption edge (7.111 keV), respectively. It is noted that the $f'(E)$ values are –2.884 at 6.811 keV and –5.368 at 7.086 keV for Fe, respectively.

The network structure consisting of FeO_6 octahedra corresponding to the middle-range ordering was estimated using the RMC simulation technique. In this simulation, we started with an initial configuration of 4320 particles, iron atom = 1440 and oxygen atom = 2880 in a volume of 3.76 x 3.88 x 3.68 nm^3, positioned along the way similar to an ideal structure of γ-FeOOH, in a super cell and the computed interference functions were compared with two independent experimental data of the ordinary and environmental interference functions. A new configuration is then generated by the random movement of particles and the interference functions are computed. Such iterative process is made until we get a reasonable convergence /10,11/. It has also been the focusing point of this work to reveal the network structure and its distortion from the ideal case found in a typical component of corrosion products, γ-FeOOH. This includes how the alloying elements affect the structure of rust formed on the surface of iron-based alloys and commercial steel.

Figure 7 shows the differential intensity profile (top) of a rust sample obtained from two intensity profiles (bottom) by the AXS measurements using the results of rust formed on Fe-2%Cr as an example /10/. Such differential intensity profiles obtained in different samples in a similar manner were used for analyzing the environmental interference functions for Fe. On the other hand, Fig. 8 gives the interference functions of five samples obtained from diffraction measurements using Mo Kα radiation /10/. It may be worth mentioning here that the present rust samples consist mainly of γ-FeOOH for all five cases, although a few signals of other components such as α-FeOOH and Fe_3O_4 are detected.

Figure 9 shows the radial distribution functions

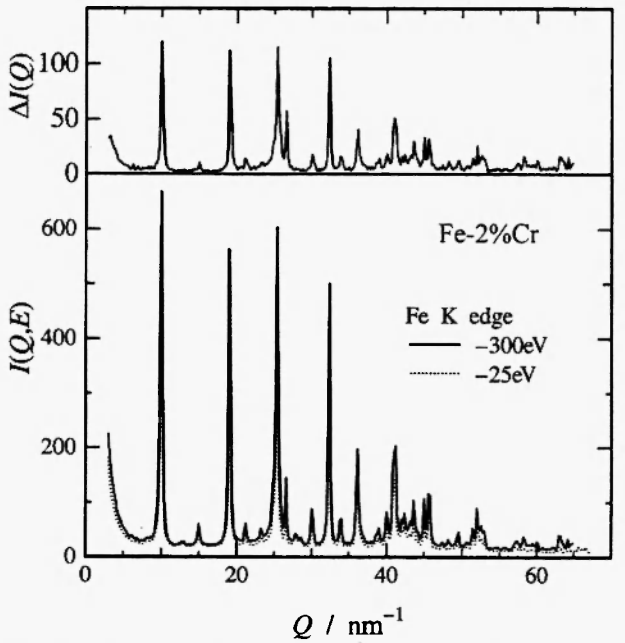

Fig. 7: Differential intensity profile (top) of rust formed on Fe-2%Cr obtained from the intensity profiles (bottom) measured at two energies of 7.086 and 6.811 keV near the Fe absorption edge /10/.

(RDF) for the γ-FeOOH component formed on the surface of Fe, Fe-2%Cr, Fe-3%Ni, Fe-1.6%Cu and WS, which were obtained from the interference functions of Fig. 8 by Fourier-Transformation. These results clearly suggest there are some differences in the atomic scale structure of five rust samples by detecting changes in position, peak height and its shape. However, any definite comment about the linkage of the FeO_6 octahedral unit structure cannot be drawn from these data alone.

The realistic atomic scale structure of the γ-FeOOH component in the range of a few nanometers can be estimated by fitting the ordinary interference function $Qi(Q)$ and environmental interference functions $Q\Delta i_{Fe}(Q)$ using the RMC simulation technique. Figure 10 shows a comparison of the ordinary interference function $Qi(Q)$ and environmental interference functions $Q\Delta i_{Fe}(Q)$ for Fe using the case of Fe-2%Cr /10/. Open circles denote the experimental data and solid lines are the results computed by the RMC simulation. The resultant middle range ordering in the γ-FeOOH component is illustrated in Fig. 11, using the

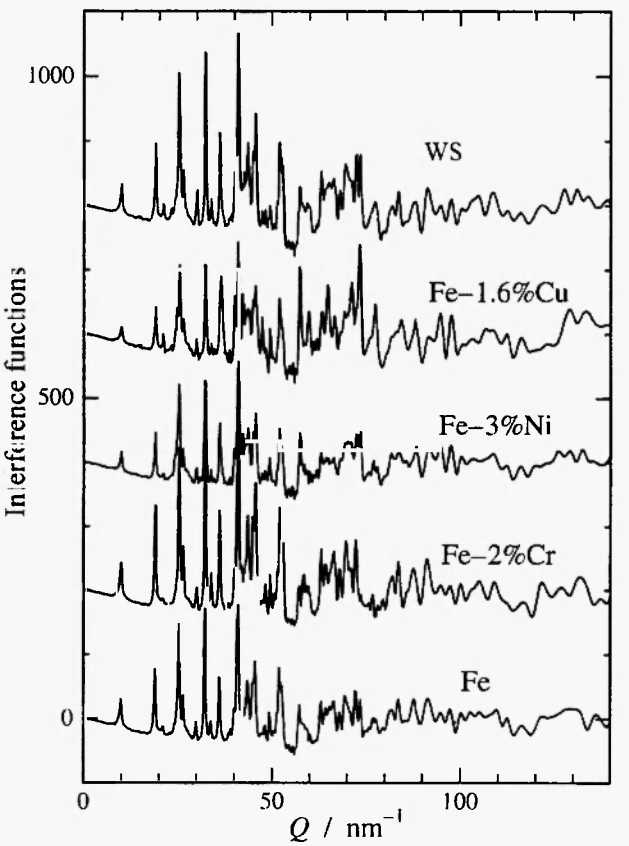

Fig. 8: Interference functions of rust formed on Fe, Fe-2%Cr, Fe-3%Ni, Fe-1.6%Cu and WS.

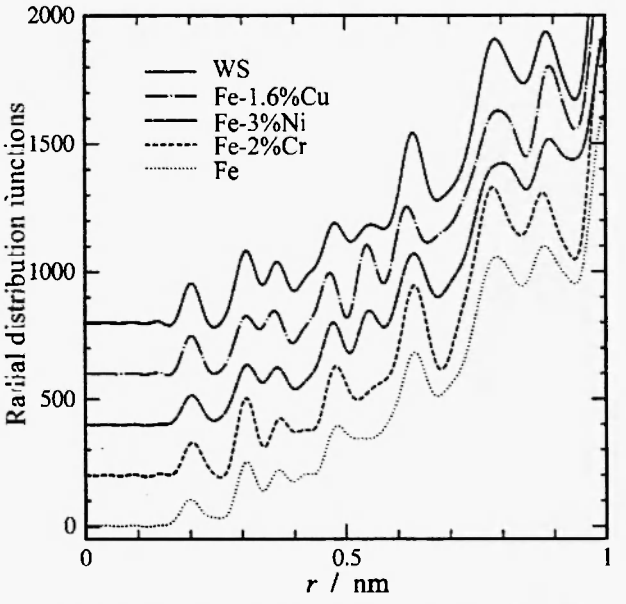

Fig. 9: Radial distribution functions of rust formed on Fe, Fe-2%Cr, Fe-3%Ni, Fe-1.6%Cu and WS.

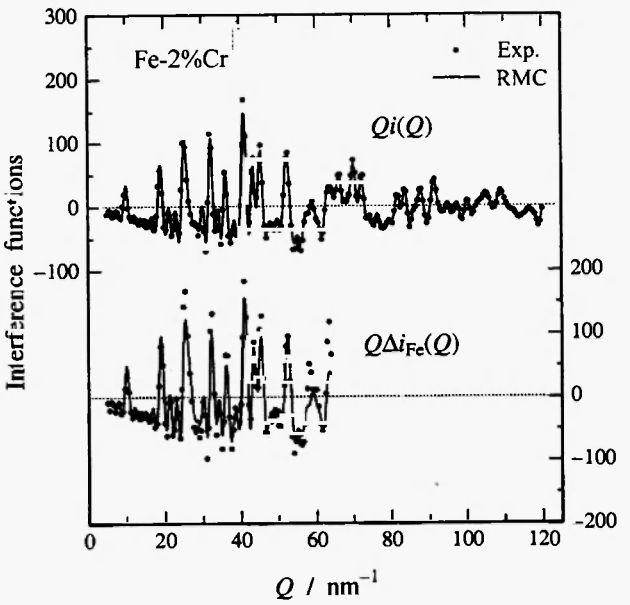

Fig. 10: The ordinary interference function $Qi(Q)$ and environmental interference functions $Q\Delta i(Q)$ for Fe of rust formed on Fe-2%Cr. Open circles and solid lines denote the experimental data and calculated values using the RMC simulation technique.

ideal γ-FeOOH structure and the γ-FeOOH component in rust formed on the surface of Fe-2%Cr. The deviation of network structure from the ideal γ-FeOOH is clearly observed and it has been quantified in the γ-FeOOH component in rust formed on the surface of Fe-2%Cr. Such RMC simulation was made in another four cases; Fe, Fe-3%Ni, Fe-1.6%Cu and WS. Then, the realistic atomic scale structure of the γ-FeOOH component in five rust samples formed on the different alloy surface has been visualized and the results are summarized in Fig. 12. It would be very interesting to note that the atomic scale structure of the γ-FeOOH component in rust significantly dependent on the composition of substrate materials.

A new method for visually displaying the deviation of the FeO_6 network structure from the ideal γ-FeOOH case has also been proposed by interpreting two parameters /10/: a bond angle between different orientations of two iron atoms in the network of the FeO_6 octahedral unit structure, θ, and a distance between the two Fe-Fe pairs, r, as shown in Fig. 13. In the ideal case of γ-FeOOH, the bond angle θ can be found at about 0, 60, 90 and 120 degrees. The present authors

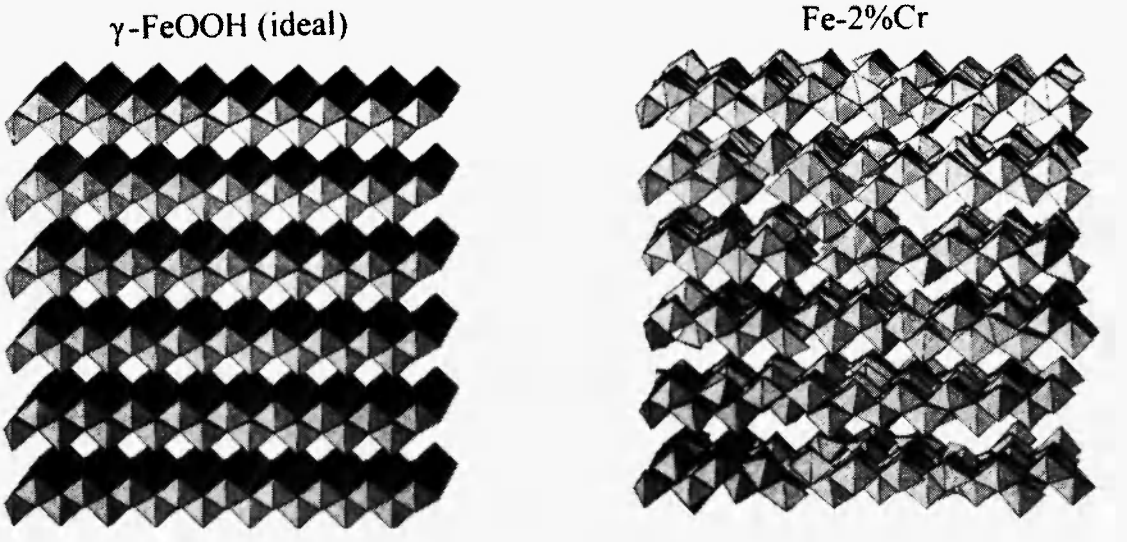

Fig. 11: A projection of the atomic positions in the middle range ordering from a representative RMC-generated configuration for rust (b) formed on the Fe-2%Cr surface. The ideal structure found in γ-FeOOH is also given in (a) as a reference. Here, the FeO_6 octahedral unit structure is employed for presentation.

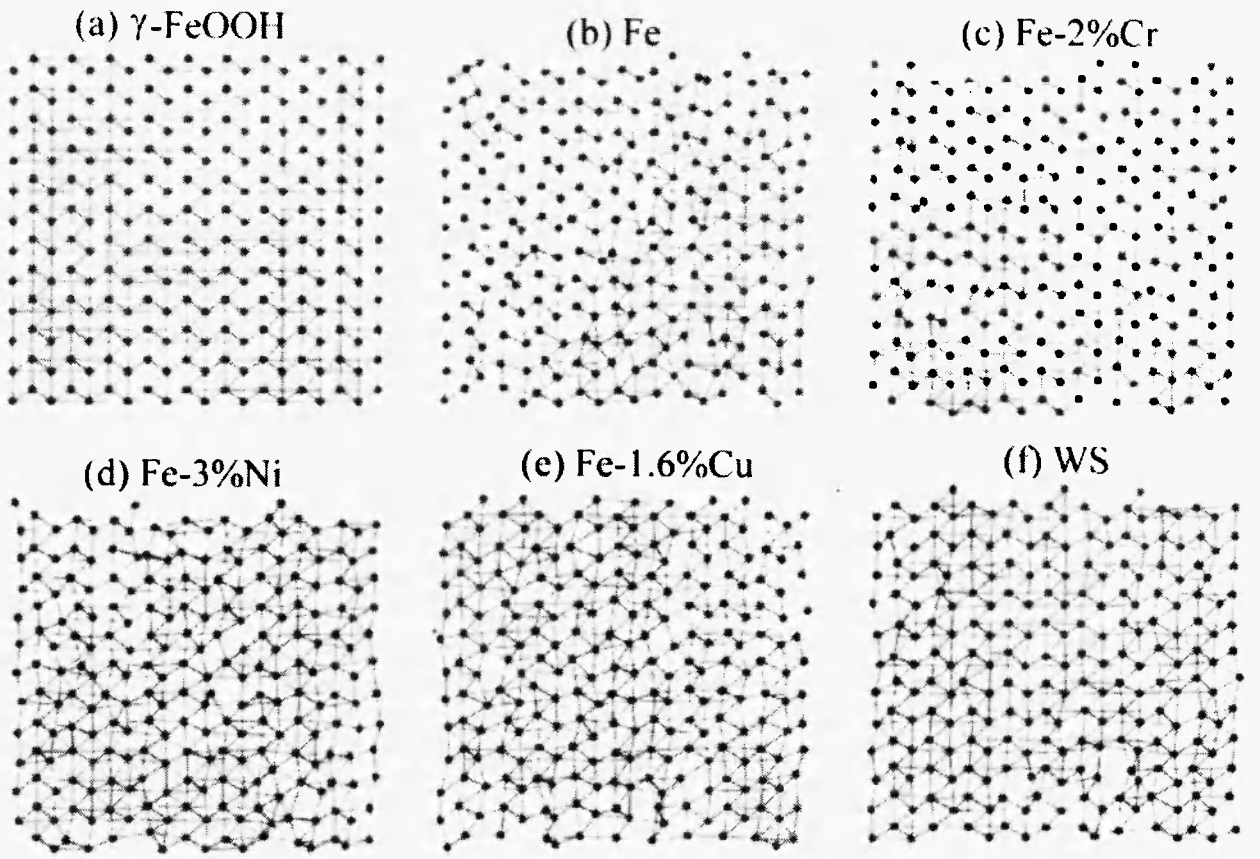

Fig. 12: A projection of the atomic positions in the middle range ordering from a representative RMC-generated configuration for five rust samples. Here, bonds between nearest neighbor Fe atoms are drawn by sticks. (a) ideal γ-FeOOH, (b)Fe, (c)Fe-2%Cr, (d)Fe-3%Ni, (e)Fe-1.6%Cu and (f)WS.

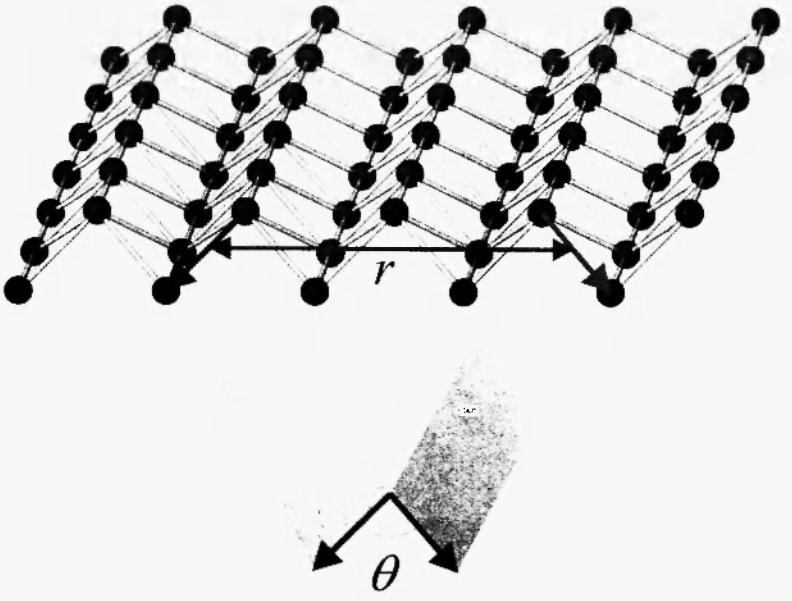

Fig. 13: Schematic diagram for analyzing the network structure of rust by estimating bond angle distribution $B(\theta,r)$ between Fe-Fe pairs.

maintain the view that the bond angle distribution defined by $B(\theta,r)$ between Fe-Fe pairs as a function of angle θ and distance r is one useful way to represent the deviation of the network structure from the ideal case. The results are summarized in Fig. 14 /10/. From this systematic information on the middle range ordering of the γ-FeOOH component in rust formed on the surface of iron-based alloys and commercial steel, the distortion of the FeO_6 octahedral units and their network structure from the ideal γ-FeOOH case is summarized in Fig. 15.

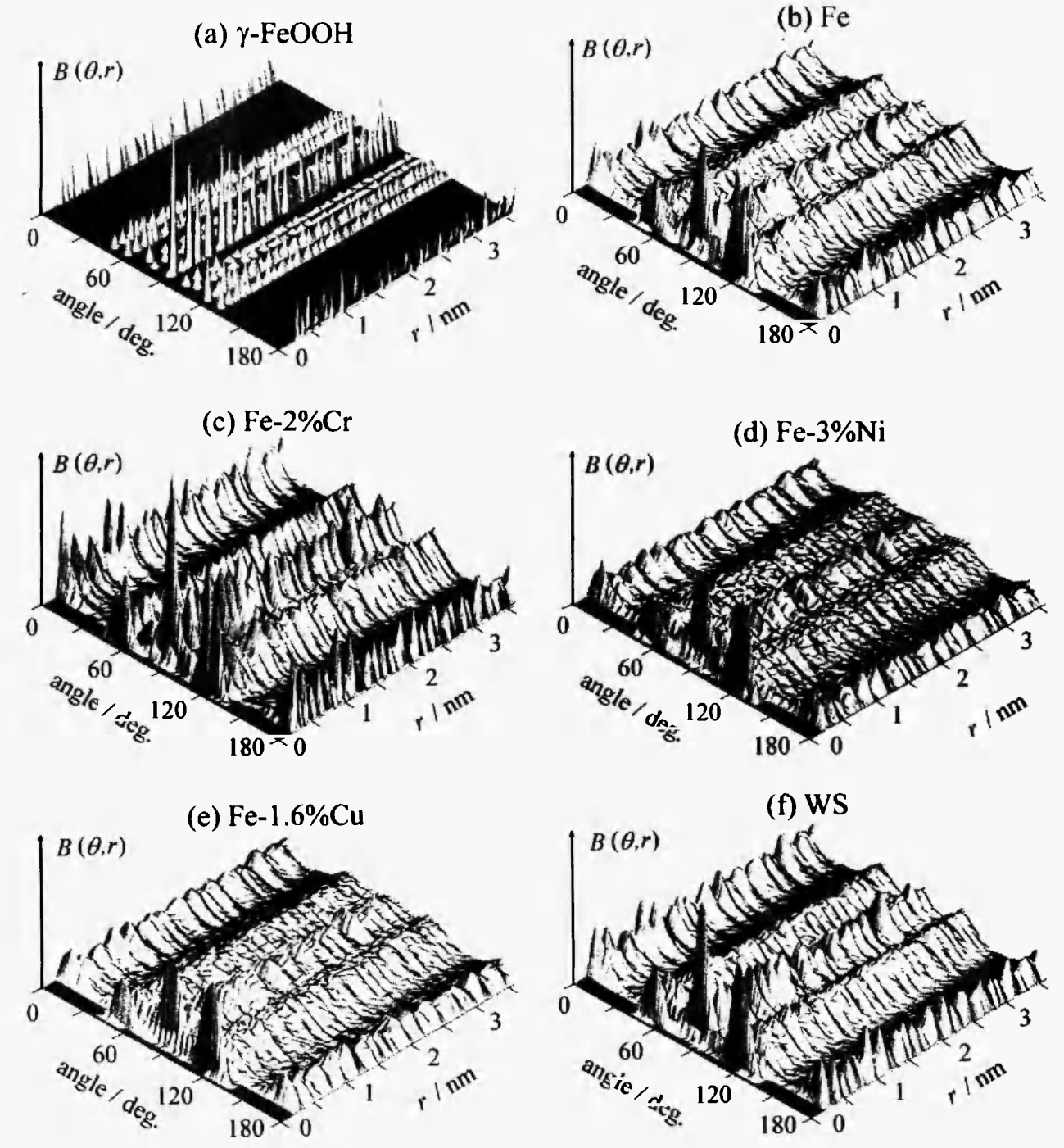

Fig. 14: Bird views of bond angle distribution $B(\theta,r)$ between Fe-Fe pairs for five rust samples. (a) ideal γ-FeOOH, (b)Fe, (c)Fe-2%Cr, (d)Fe-3%Ni, (e)Fe-1.6%Cu and (f)WS.

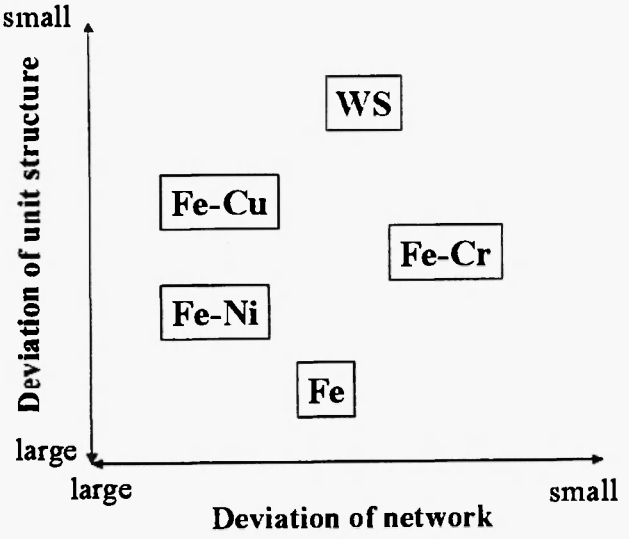

Fig. 15: Schematic representation of relationships between deviation from the ideal case with respect to the fundamental unit structure and the network structure for five rust samples.

The atomic scale model structure of the γ-FeOOH component in rust formed on iron based alloys and weathering steel has been estimated and it is quite likely to be represented by the distortion of the FeO_6 octahedral units and their network structure. Such features are found to depend on the composition of substrate materials. This implies that an alloying element, more or less, occupies a certain site of the FeO_6 unit structure formed during corrosion and such occupation may affect not only on the short range ordering but also on the middle range ordering characterized by the FeO_6 octahedral units. Figure 16 shows the results on the middle range ordering recently obtained for two synthesized α-FeOOH samples containing chromium /11/. The linkage of the FeO_6 and CrO_6 octahedral unit structures is cited in α-FeOOH with 29 % Cr and the distortion in linkage of these octahedral unit structures is considered to result from the substitution of iron for chromium in the α-FeOOH structure. Thus, it is not too much to say that the alloying elements play an important role in the formation processes of the atomic scale structure of rust, although hydrogen in the rust structure, which has not yet been clarified, may also be important.

Within the best knowledge of the present authors, systematic differences in the atomic scale structure of rust formed on iron and steel were quantified for the first time. The method described in this work is

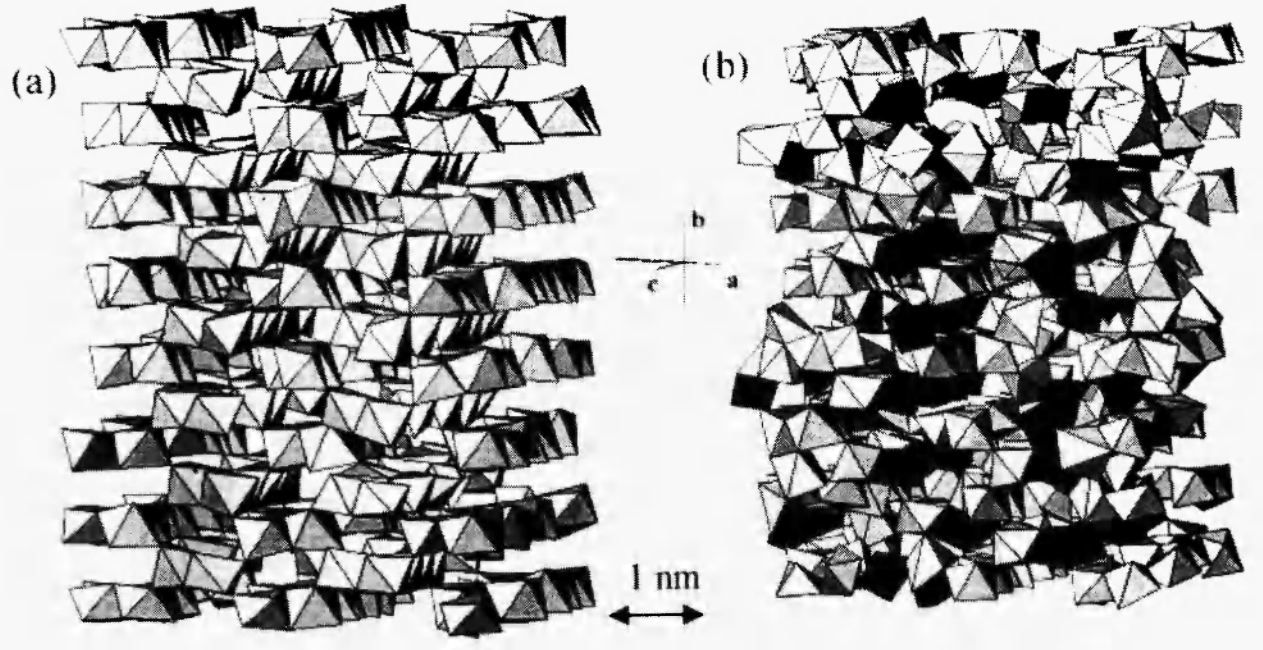

Fig. 16: A projection of the atomic positions in the middle range ordering from a representative RMC-generated configuration for (a) α-FeOOH and (b) α-29Cr. visualized by the FeO_6 octahedral unit structure. The CrO_6 octahedral units in α-29Cr are denoted as dark octahedron in (b) /11/.

considered to be one way to reduce the difficulty in materials characterization of corrosion products, which is still a matter of controversy. Although only quantitative analyses of the atomic scale structure in the γ-FeOOH component of rust formed in salt water has been made, it would be very interesting to extend the present method to other rust components such as α-FeOOH and Fe_3O_4. By a series of such structural analyses together with corrosion experiments, the condition for designing protective rust layers on low-alloyed steel may be optimized.

5. CONCLUDING REMARKS

Anomalous X-ray scattering (AXS) coupled with the reverse Monte-Carlo (RMC) simulation technique has been used for obtaining the realistic atomic scale model structure including the middle range ordering. The usefulness of this new method was confirmed by obtaining some interesting structural information, which is not sufficiently represented yet, with respect to a complex system such as molten CuBr and corrosion products (ferric oxyhydroxides, such as FeOOH) formed on the steel surface. This method would be valuable for materials characterization not only of non-crystalline systems but also of crystalline systems in the variety of states.

On the other hand, it should be kept in mind that the present method coupled with the RMC simulation technique is not a unique mathematical procedure. Nevertheless, the resultant model structure obtained by fitting two or three independent experimental data is considered, at least, in a sense of the necessary condition although it might be not the sufficient condition. For this reason, we believe that the present method is one way to obtain the realistic atomic scale model structure in the range of a few nanometers within the framework of information in a sense of necessary condition at best. Thus, it would be very promising to extend this method to the estimation of the middle range ordering of various systems, so that its validity may be tested on a wider base.

This work was supported by the Grant-in-Aid for Scientific Research Fund from the Japan Society for Promotion of Science (No 15656152). A part of this work was also supported by a research promotion grant of The Iron and Steel Institute of Japan.

REFERENCES

1. T.L. Hill, *Statistical Mechanics*, Mc-Graw Hill, New York, 1956.
2. A. Inoue, *Bulk Amorphous Alloys*, Trans. Tech. Uetkon-Zürich, 1999.
3. T. Misawa, K. Asami, K. Hashimoto and S. Shimodaira, *Corros. Sci.*, **14**,279(1974).
4. H. Okada, Y. Hosoi, K. Yukawa and H. Narita: *Iron Steel Inst. Jpn.*, **55**,355 (1969).
5. R.L. McGreevy and L. Pusztai, *Mol. Simul.*, **1**, 359(1988).
6. R.L. McGreevy and L. Pusztai, *Proc. Roy. Soc. London*, **A430**, 241 (1990).
7. M. Saito, C.Y. Park, K. Omote, K. Sugiyama and Y. Waseda: *J. Phys. Soc. Jpn.* , **66**, 633 (1997).
8. M. Saito, S.C. Kang and Y. Waseda, *J. Appl. Phys. Suppl.*, **38**, 596 (1999).
9. M. Saito, C.Y. Park, K. Sugiyama and Y. Waseda: *J. Phys. Soc. Jpn.*, **66**, 3120 (1997).
10. S. Suzuki, M. Saito, M. Kimura, T. Suzuki, H. Kihira and Y. Waseda, *ISIJ Inter.*, **43**, 336 (2003).
11. Y. Waseda, S. Suzuki and M. Saito, *J. Alloy Compound*, (2004), in press.
12. Y. Waseda, *Anomalous X-ray Scattering for Materials Characterization*, Springer, Heidelberg, 2002.
13. J.E. Enderby, D.M. North and P.A. Egelstaff, *Phil. Mag.*, **14**, 961 (1966).
14. C.N.J. Wagner, *Liquid Metals, Chemistry and Physics* edited by S. Z. Beer, Marce-Dekker, New York, 1972, p. 258.
15. F.G. Edwards, J.E. Enderby, R.A. Howe and D.I. Page, *J. Phys. C.*, **8**, 3483 (1975).
16. T.E. Faber and J.M. Ziman, *Phil. Mag.*, **11**, 153 (1965).
17. R.W. James, *The Optical Principles of the Diffraction of X-rays*, G. Gell, London, 1954.
18. P. Hagenmuller and W. van Goal (editors), *Solid Electrolytes*, Academic Press, New York, 1978.

19. *International Tables for X-ray Crystallography, Vol. IV*, edited by J.A. Ibres and W.C. Hamilton, Kynoch, Birmingham, 1974.
20. M. Inui, S. Takeda and T. Uechi, *J. Phys. Soc. Jpn.*, **60**, 3190 (1991).
21. Y. Shirakawa, M. Saito, S. Tamaki, M. Inui and S. Takeda, *J. Phys. Soc. Jpn.*, **60**, 2687 (1991).
22. Y. Waseda, *The Structure of Non-Crystalline Materials*, McGraw-Hill, New York, 1980.
23. D.I. Page and I. Mika, *J. Phys. C.*, **4**, 3034 (1971).
24. S. Eisenberg, S.F. Jal, J. Dupuy, P. Chieux and W. Knoll, *Phil. Mag. A.*, **46**, 195 (1982).
25. R. G. Stantoson, *Numerical Methods for Science and Engineering*, Prentice-Hall, New York, 1961.
26. T. Misawa, M. Yamashita, K. Matsuda, H. Miyuki and J. H. Nagano, *Iron Steel Inst. Jpn.*, 79, 69 (1993).
27. M. Yamashita, H. Miyuki, Y. Matsuda, H. Nagano and T. Misawa, *Corrosion Sci.*, **36**, 283 (1994).
28. T. Okada, Y. Ishii, T. Mizoguchi, I. Tamura, Y. Kobayashi, Y. Takagi, S. Suzuki, H. Kihira, M. Itoh, A. Usami, K. Tanabe and K. Masuda, *Jpn. J. Appl. Phys.* **39**, 3382 (2000).
29. T. Kamimura, S. Nasu, T. Tazaki, K. Kuzushita and S. Morimoto, *Materials Trans.* **43**, 694 (2002).
30. T. Kamimura, S. Nasu, T. Segi, T. Tazaki, S. Morimoto and H. Miyuki, *Corros. Sci.*, **45**, 1863 (2003).
31. M. Yamashita, T. Shimizu, H. Konishi, J. Mizuki and H. Uchida, *Corros. Sci.* **45**, 381 (2003).
32. S. Suzuki, Y. Takahashi, T. Kamimura, H. Miyuki, Y. Takagi, K. Shinoda, K. Tohji and Y. Waseda, *Corros. Sci.*, **46**, 1751 (2004).